

# Jet energy scale calibration in the D0 experiment

**Jeroen Hegeman**

Nikhef, Kruislaan 409, 1098 SJ Amsterdam, The Netherlands

E-mail: [jhegeman@nikhef.nl](mailto:jhegeman@nikhef.nl)

**Abstract.** Using the Run IIa data set the D0 experiment has reached a jet energy calibration precision on the level of 1–2% over a wide kinematic range. This paper presents the methods used and the results obtained. Special attention is paid to the remaining systematic uncertainties.

Most physics analyses at hadron colliders involve multiple jets, making the calibration of the jet energy scale an important input. Since many of the results based on the Tevatron Run IIa data set are limited by systematic uncertainties, any improvements in jet energy scale translate directly into improved precision of the published results.

## 1. The D0 detector

The D0 detector [1, 2] is a general purpose detector designed for the study of high- $p_T$  effects in proton-antiproton collisions. Situated in the Fermilab Tevatron collider ring, during Run IIa it collected approximately  $1 \text{ fb}^{-1}$  of data at  $\sqrt{s} = 1.96 \text{ TeV}$ .

The D0 detector uses a uranium-liquid argon sampling calorimeter system (figure 1) consisting of a central calorimeter covering the pseudorapidity region  $|\eta| \lesssim 1.1$  and two endcap calorimeters extending the range to  $|\eta| \lesssim 4.2$ . Both central- and endcap calorimeters are housed in individual cryostats. The region between central- and endcap cryostats ( $1.1 \lesssim |\eta| \lesssim 1.4$ ) is instrumented with a scintillator based inter-cryostat detector. The cell based readout provides a transverse segmentation of  $\Delta\eta \times \Delta\phi = 0.1 \times 2\pi/64$  up to  $|\eta| = 3.2$ . More forward the cell size increases to avoid too small cells. The electromagnetic calorimeter consists of four layers with a total thickness of  $\approx 20 X_0$ . The third EM layer, around the approximate electromagnetic shower maximum, is segmented twice as finely in both  $\eta$  and  $\phi$  directions. The hadronic calorimeter contains three (central) or four (endcaps) fine hadronic layers followed by a coarse hadronic layer (using copper and stainless steel absorbers instead of uranium). The total depths of the central- and endcap hadronic calorimeters are  $\approx 7.2 \lambda$  and  $8.0 \lambda$  respectively. A scintillating fiber preshower detector covers the range  $|\eta| < 1.3$ . Preshower information is used both in EM cluster reconstruction and in photon identification. Intercalibration of the D0 calorimeter in rings of  $\phi$  has been performed using  $Z \rightarrow e^+e^-$  and QCD di-jet events [3]. The D0 detector simulation is based on the GEANT package.

## 2. Jet reconstruction

Jets are reconstructed using the ‘Run II midpoint cone algorithm’ [4]. Cells with the same  $\eta/\phi$  coordinates are combined into pseudo-projective towers (figure 1b). Starting from seed towers, calorimeter towers within a cone of radius  $\Delta\mathcal{R} = \sqrt{(\Delta y)^2 + (\Delta\phi)^2} < \mathcal{R}_{\text{jet}}$  around the seed are clustered. The jet axis is determined by four-vector addition of the clustered towers. This process

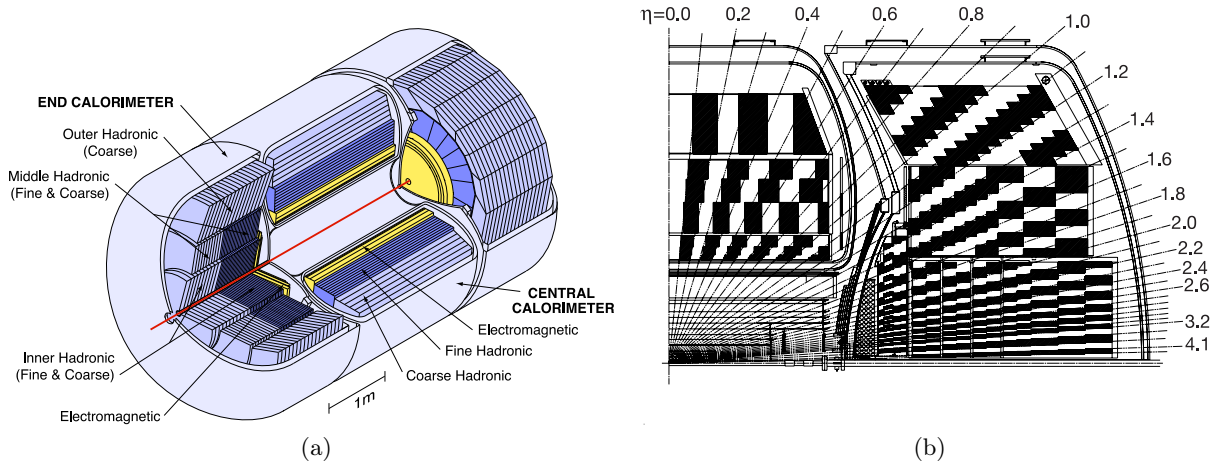


Figure 1: (a) Isometric view and (b) beam-parallel view of a portion of the D0 calorimeter system. The shading patterns indicate the calorimeter segmentation.

is repeated until the jet axis is stable. The midpoints between jet pairs are used as additional seeds to improve infrared safety. Identical solutions are removed and, depending on the amount of overlap, overlapping jets are either split or merged into a single jet. Two different cone sizes are used: 0.5 and 0.7 and the jet reconstruction threshold is  $p_T \geq 6 \text{ GeV}/c$ . By using stable Monte Carlo particles instead of calorimeter towers the exact same jet reconstruction algorithm can be applied in simulation.

### 3. Jet energy scale corrections

Typically, physics analyses depend on data-to-Monte Carlo comparisons of reconstructed physics objects. To allow for such comparisons the jet energy scale corrects the jet energy as measured in the calorimeter back to the jet energy as reconstructed at the stable-particle level.

To avoid depending on the possibly imperfect detector simulation, especially considering the modified Run II detector geometry compared to the pre-Run I testbeam data, a data-driven calibration procedure is employed. Any Monte Carlo used employs a tuned version of the PYTHIA event generator.

The subcorrections making up the jet energy scale correction (eq. (1)) are (i) the offset subtraction  $O$  removing spurious energy, (ii) the absolute ( $R$ ) and  $\eta$ -dependent ( $F_\eta$ ) response and (iii) the out-of-cone showering corrections  $S$  correcting for lateral energy leakage out of the jet cone. Each subcorrection is calibrated individually and possible method biases are taken into account explicitly where necessary.

$$E_{\text{jet}}^{\text{ptcl}} = \frac{E_{\text{jet}}^{\text{meas}} - O}{F_\eta \cdot R \cdot S} \quad (1)$$

It should be noted that the underlying event, consisting of the beam remnants and their connections with the hard scatter constituents, is an integral part of the physics process and neither can nor should be corrected for in the energy calibration procedure.

#### 3.1. Offset subtraction

The offset correction subtracts all energy from the jet cone that is not related to the hard scatter event. Contributions from (both electronics and uranium) noise and pile-up energy from previous

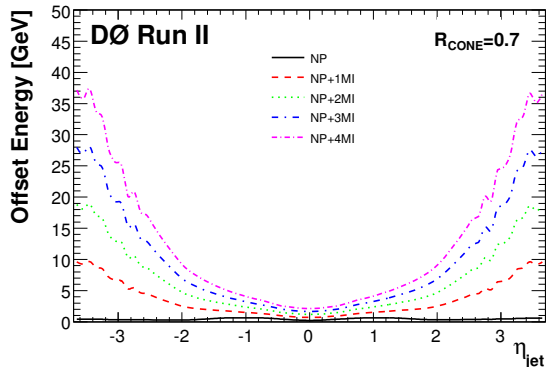


Figure 2: The noise/pile-up (NP) and multiple interactions (MI) contributions to the offset energy as a function of jet pseudorapidity for  $\mathcal{R}_{\text{jet}} = 0.7$  cone jets.

bunch crossings is separated from the effects of possible additional proton-antiproton interactions. The noise/pile-up contribution is estimated from zero-bias data, data triggered on the presence of a bunch crossing, vetoed for inelastic interactions. Energy depositions due to multiple interactions are estimated from minimum-bias data: data triggered on the presence of a (possibly inelastic) interaction. The overall energy difference between minimum-bias events with  $N_{\text{PV}}$  reconstructed vertices and single vertex events is considered as the energy originating from  $N - 1$  additional interactions:

$$\text{MI}(N_{\text{PV}}) = \text{MinBias}(N_{\text{PV}}) - \text{MinBias}(N_{\text{PV}} = 1)$$

The 396 ns bunch crossing separation together with the high instantaneous luminosities delivered by the Tevatron result in a Poisson-distributed average number of up to five simultaneous proton-antiproton collisions per beam crossing. This implies that most events contain at least one interaction in addition to the hard scatter under study.

Both noise/pile-up and multiple interactions corrections are estimated as average energies over rings in  $\phi$  for each  $\eta$ -ring of towers. This is translated to a per-jet offset correction (figure 2) based on the position of the jet axis and the cone size.

Calorimeter information is zero-suppressed: cells with negative energies or with a signal within  $2.5 \sigma$  from their noise pedestals are dropped from the readout. The presence of jet energy thus locally increases the noise survival level leading to an underestimation of the offset energy inside jets. This effect is largely counteracted by the fact that photons, due to their small shower sizes, are less than jets affected by the zero-suppression, leading to a slight underestimate of the response. These two effects were studied in detail in Monte Carlo. The remaining effect is of the order of 1.5% below  $p_{\text{T}} \approx 50 \text{ GeV}/c$  and is incorporated in the combined jet energy corrections.

### 3.2. Response corrections

The presence of the inner trackers, solenoid and preshower detector corresponds to a significant amount of material in front of the calorimeter:  $\approx 4.0 X_0$  at normal incidence, rising to  $\approx 4.4 X_0$  in the endcaps at  $\eta = 2$ . To reduce pile-up effects signal integration is restricted to the first  $\approx 260 \text{ ns}$  of each crossing. Compared to the  $\approx 450 \text{ ns}$  typical drift time in the liquid argon gaps this means only two thirds of the charge is collected. The result is a strongly non-compensating calorimeter:  $e/h > 1$ , making the response corrections by far the largest contribution to the overall jet energy scale.

**3.2.1. The MPF method** The MPF (missing  $E_{\text{T}}$  projection fraction) method uses the fact that in back-to-back tag-and-probe events tag and probe are perfectly balanced at the particle

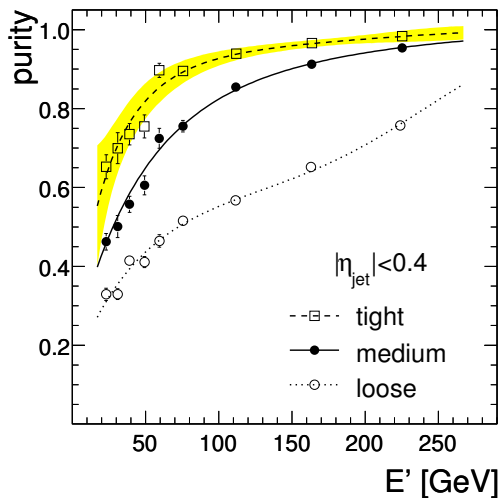


Figure 3: The purity of the photon+jet data sample used for response corrections estimated for three different photon selection criteria (loose, medium and tight). The band surrounding the curve corresponding to the tight photon selection corresponds to the total uncertainty on the photon purity.

level. Starting from a calibrated tag, any miscalibration of the probe will be reflected in missing transverse energy. The detector response to the probe can be expressed as:

$$R_{\text{probe}} = 1 + \frac{\vec{E}_{\text{T}} \cdot \vec{p}_{\text{T, tag}}}{p_{\text{T, tag}}^2}.$$

To suppress the effects of the jet energy resolution all response corrections are parameterized versus the expected jet energy  $E' \equiv p_{\text{T, tag}} \cosh \eta_{\text{jet}}$ .

*3.2.2. Absolute calorimeter response* A photon+jet event sample using central photons ( $|\eta| < 1.0$ ) is used to estimate the response of central jets ( $|\eta| < 0.4$ ). The tag photon and probe jet are required to be tightly back-to-back:  $\Delta\phi > 3.0$ . The photon selection criteria include stringent cuts on the fraction of energy deposited in the EM calorimeter, shower shape information in the third EM layer and the preshower detector, as well as both track- and calorimeter based isolation cuts. Nevertheless the photon+jet sample contains a significant fraction of QCD di-jet contamination, typically due to jets with leading neutral pions. The photon purity was estimated for three different photon selection criteria (figure 3) in both Monte Carlo and data (using a template based method). Measured purities in data and MC were found to be in excellent agreement [5]. Corrections for di-jet contamination were studied in all three samples, bringing the response back to the same value in all cases. The final response correction (figure 4a) is based on the tight photon selection, giving the highest purity and the smallest purity correction. The uncertainties on the response (figure 4b) are dominated by the photon purity (low  $p_{\text{T}}$ ) and the photon energy calibration (above  $p_{\text{T}} \gtrsim 30$  GeV/c). It should be noted that the response corrections are known to a precision of  $\approx 1.3\%$  up to the highest jet energies.

The MPF method balances the full hadronic recoil against the tag photon under the assumption that the jet fully contains the hadronic recoil. It is thus sensitive to additional energy in the event, e.g. jets below the reconstruction threshold. The effects of the reconstruction threshold, the choice of the  $\Delta\phi$  back-to-backness cut and different underlying event models were studied in Monte Carlo where individual energy depositions can be compared to the true energies. The residual correction is of the order of  $\approx 2\%$  and is incorporated into the combined jet energy scale corrections.

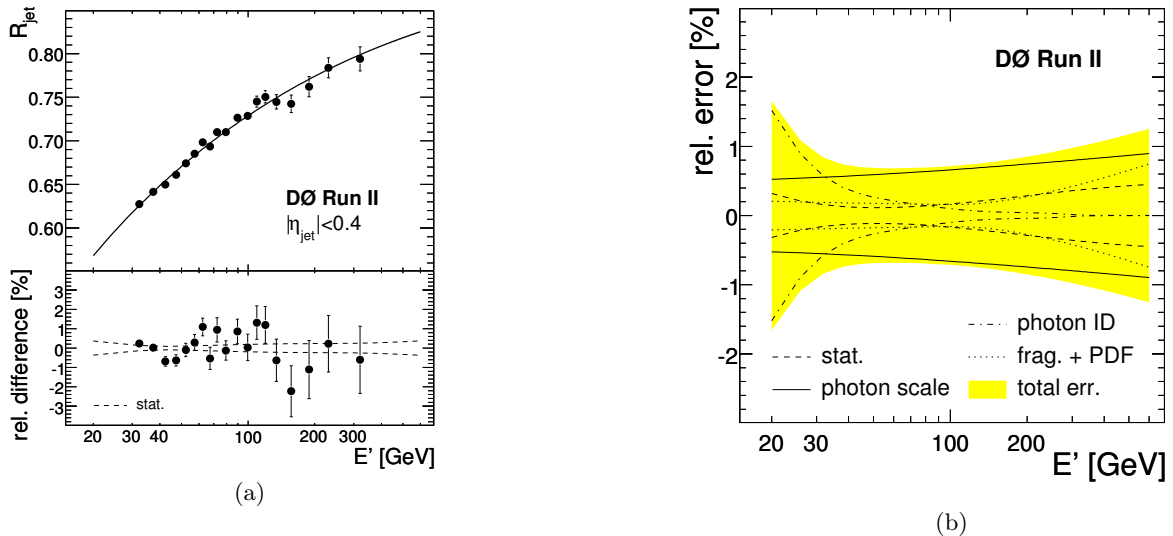


Figure 4: (a) The fitted absolute response for central  $\mathcal{R}_{\text{jet}} = 0.7$  cone jets. The bottom inset shows the fit residuals and the statistical uncertainty on the fit. (b) The systematic uncertainties affecting the absolute response ( $|\eta| < 0.4$ ). Except at low  $p_T$  the propagation of the photon energy calibration is the dominant contribution.

**3.2.3.  $\eta$ -Dependent response corrections** While the D0 calorimeter is fairly uniform within the central- and endcap regions the gaps between the cryostats are instrumented differently. Also, the amount of dead material depends on jet pseudorapidity.

The relative response correction calibrates forward jets with respect to central jets. Together with the absolute detector response this provides the response correction for forward jets.

The relative response is measured using the MPF method on both photon+jet and di-jet samples. The tag photon (jet) is required to be within  $|\eta| < 1.0$  ( $|\eta| < 0.4$ ), the probe jet is unrestricted in pseudorapidity. Tag and probe are required to be back-to-back:  $\Delta\phi > 3.0$ . The di-jet sample reaches higher in jet transverse momentum and is used to determine the shape of the response corrections at high  $p_T$ .

The different quark/gluon compositions of jets in photon+jet and di-jet events lead to different response corrections. Whereas photon+jet events at low  $p_T$  are dominated by quark jets, the gluon jet fraction increasing with increasing  $p_T$ , di-jet events show the opposite behavior. Gluon jets tend to be wider, containing more particles with a correspondingly lower average particle energy. Both the tracker magnetic field as well as the presence of dead material lower the response of low energy particles, resulting in an overall lower response for gluon- than for quark jets (figure 5). Since forward jets traverse more material before reaching the calorimeter, this effect becomes stronger for jets in more forward regions.

Figure 6 shows a summary of the relative response corrections for  $\mathcal{R}_{\text{jet}} = 0.7$  cone jets in both photon+jet and di-jet events for a wide range of jet energies. The largest corrections are needed in the inter-cryostat regions:  $0.5 \lesssim |\eta| \lesssim 1.8$ . The influence of dead material increases at larger angles, making the relative response drop strongly in the forward direction.

The dominant systematic uncertainties result from imperfections in the parameterizations of the energy dependence and the  $\eta$ -interpolation.

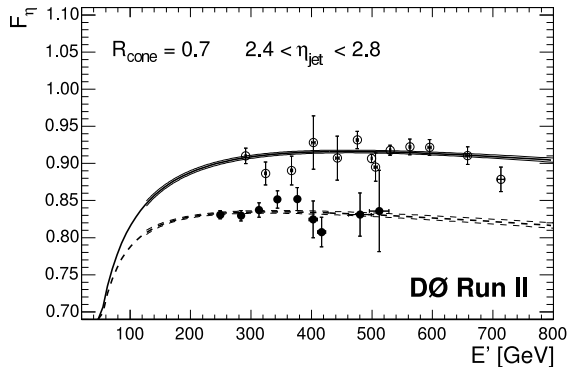


Figure 5: Relative response in data for  $\mathcal{R}_{\text{jet}} = 0.7$  cone jets within  $2.4 < |\eta| < 2.8$  for both photon+jet (bottom curve) and di-jet (top curve) events. Compared to di-jet events photon+jet events contain more gluon jets, resulting in a lower response.

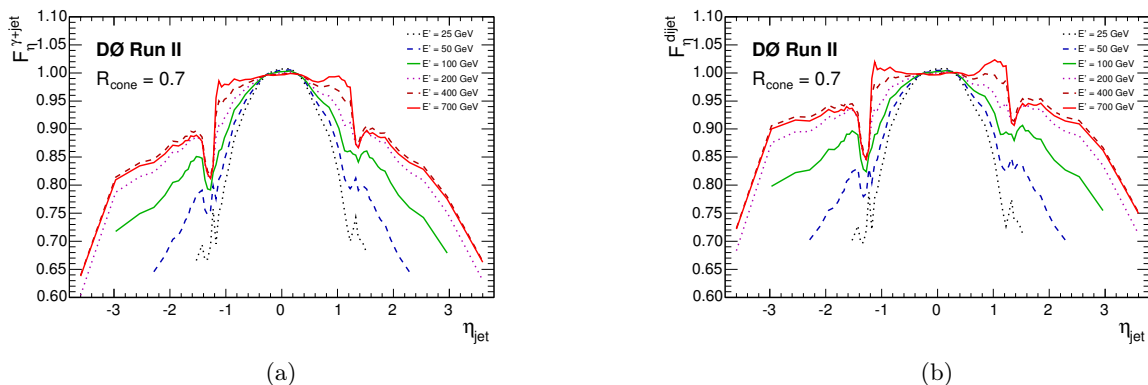


Figure 6: Relative response corrections  $F_\eta$  in data (a) for photon+jet events and (b) for di-jet events.

### 3.3. Out-of-cone showering correction

The cone jet algorithm reconstructs the jet energy as the sum of all energy present within the jet cone. Due to detector effects like particles bending in the magnetic field as well as parts of the shower leaving the jet cone in the calorimeter, the energy inside the cone may differ from the true jet energy. The out-of-cone showering correction corrects for the net energy difference due to these detector showering effects.

Using back-to-back photon+jet events in Monte Carlo without any noise and/or multiple interactions the energy deposited by each particle can be tracked in the detector simulation. Distinguishing between particles assigned to the particle level jet and other particles allows for the creation of jet- and non-jet energy deposition profiles as a function of the radial distance  $\Delta\mathcal{R}$  away from the jet axis. After offset subtraction a template fit to the data is used to estimate the true energy distributions from particles inside/outside the jet (figure 7). The net showering correction can be obtained from the jet- and non-jet energy profiles after the fit:

$$S = \frac{\int_0^{\mathcal{R}_{\text{jet}}} (E(\text{jet}) + E(\text{non-jet}))}{\int_0^\infty E(\text{jet})}$$

Since the out-of-cone showering correction is dominated by edge effects the correction becomes larger for smaller jet cone sizes. Similarly the correction becomes more prominent for jets at

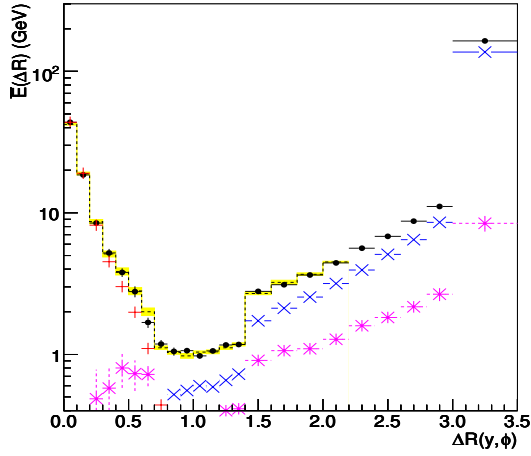
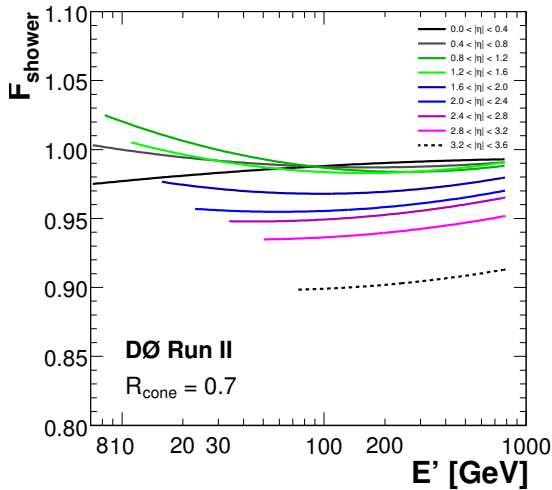
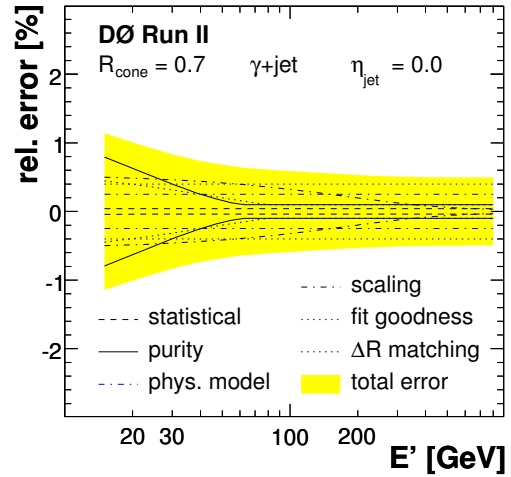


Figure 7: The jet- (+) and non-jet (x) energy distributions fitted to data for central  $\mathcal{R}_{\text{jet}} = 0.7$  cone jets ( $|\eta| < 0.4$ ) of  $100 < p_T < 130$  GeV/c. The full circles show the data, the dashed line the template the sum of the fitted energy templates. The shaded band around the fit results reflects the statistical fit uncertainty. The offset energy profile (\*) is kept fixed in the fitting.



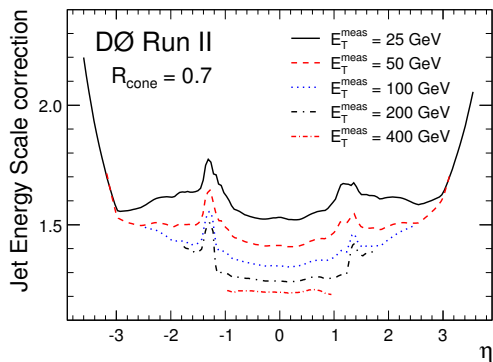
(a)



(b)

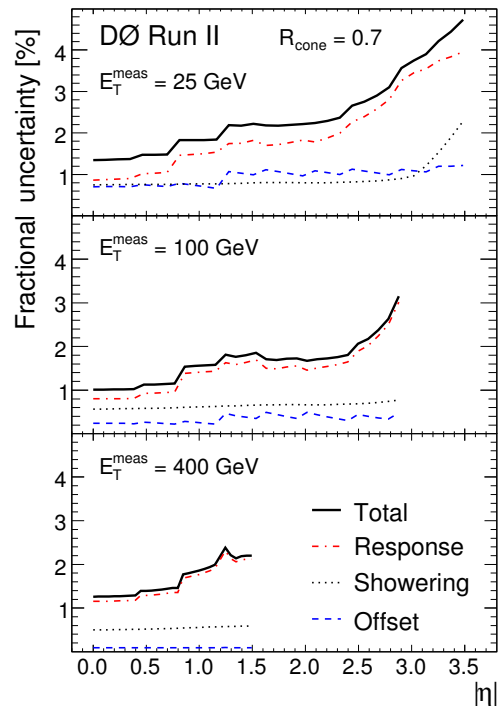
Figure 8: (a) Out-of-cone showering corrections for  $\mathcal{R}_{\text{jet}} = 0.7$  cone jets in different pseudorapidity ranges and (b) the systematic uncertainties for central jets. The dominant uncertainties are all related to the shape of the jet energy distribution profile and its agreement with the data. The uncertainty marked ‘scaling’ reflects the effect of down-scaling the single pion response in Monte Carlo to match the low- $p_T$  jet response between data and Monte Carlo.

larger pseudorapidities where the physical size of jets decreases (figure 8a). The dominant systematic uncertainties to the out-of-cone showering corrections (figure 8b) are all related to the dependability of the jet energy profile. Impurities in the photon+jet sample modify the relative quark/gluon content which is translated directly into the shape of the jet profile. The same holds true for the underlying physics models for fragmentation and hadronisation as well as for the underlying event modeling. Uncertainties due to these effects were studied in Monte Carlo. A uniform uncertainty was added to account for the differences in fit agreement over the different pseudorapidity ranges.



(a)

Figure 9: Total energy scale corrections for  $\mathcal{R}_{\text{cone}} = 0.7$  cone jets figure 9a and the corresponding relative uncertainties figure 10b (total: solid line) split into contributions from offset (dashed line), response (dash-dotted line) and showering (dotted line) corrections



(b)

#### 4. Combined jet energy scale corrections

Figure 9 shows the combined jet energy scale corrections and the corresponding uncertainties. Over a wide kinematic range the uncertainties are of the 1–2% level. All subcorrections are known to the same level of relative precision. Due to the size of the response correction this becomes the dominant uncertainty on the combined jet energy scale. At low  $p_T$  the uncertainty is dominated by the purity of the photon+jet sample. At the high  $p_T$  end the uncertainties are affected by decreasing statistics in the di-jet sample. Overall the limiting factors are the photon purity and the electromagnetic energy calibration.

The high precision jet energy calibration is directly visible in physics results. An example is the recent measurement of the inclusive jet cross section to a precision of  $\approx 10\%$  [6].

#### Acknowledgments

The results presented here are the outcome of many long term efforts of the D0 jet energy scale group and would not have been possible without the support of the whole D0 collaboration. The author would also like to thank the Stichting voor Fundamenteel Onderzoek der Materie (FOM) in the Netherlands, as well as the organizers of the CALOR 2008 conference.

#### References

- [1] Abachi S *et al.* (D0) 1994 *Nucl. Instrum. Meth.* **A338** 185–253
- [2] Abazov V M *et al.* (D0) 2006 *Nucl. Instrum. Meth.* **A565** 463–537 (*Preprint physics/0507191*)
- [3] Peters K 2006 *AIP Conf. Proc.* **867** 17–24 (*Preprint physics/0608002*) URL <http://www.slac.stanford.edu/spires/find/hep/www?eprint=physics/0608002>
- [4] Blazey G C *et al.* 2000 (*Preprint hep-ex/0005012*) URL <http://www.slac.stanford.edu/spires/find/hep/www?eprint=hep-ex/0005012>
- [5] The D0 collaboration *Paper in preparation for Nucl. Instrum. Meth.*
- [6] Abazov V M *et al.* (D0) 2008 *Submitted to PRL* (*Preprint 0802.2400*)